

<https://doi.org/10.1038/s41528-024-00306-2>

# Deformable micro-supercapacitor fabricated via laser ablation patterning of Graphene/liquid metal

Check for updates

Keon-Woo Kim<sup>1,5</sup>, Seong Ju Park<sup>2,5</sup>, Su-Jeong Park<sup>2</sup>, Inae Kim<sup>2</sup>, Bomi Park<sup>1</sup>, Se Hyun Kim<sup>3</sup>,  
Unyong Jeong<sup>4</sup>, Jin Kon Kim<sup>1</sup>✉ & Chanwoo Yang<sup>2</sup>✉

Deformable and miniaturized energy storage devices are essential for powering soft electronics. Herein, we fabricate deformable micro supercapacitors (MSCs) based on eutectic gallium-indium liquid metal (EGaIn) current collectors with integrated graphene. The well-define interdigitated electrode patterning with controlled gap is successfully realized by using the laser ablation because of a strong laser absorption of graphene and EGaIn. By judicious control of gap size between neighboring interdigitated electrodes and mass loading of graphene, we achieve a high areal capacitance ( $1336 \mu\text{F cm}^{-2}$ ) with reliable rate performance. In addition, owing to the intrinsic liquid characteristics of EGaIn current collector, the areal capacitance of fabricated MSC retains 90% of original value even after repetitive folding and 20% stretching up to 1000 cycles. Finally, we successfully integrate deformable MSC with a commercial light-emitting diode to demonstrate the feasibility of MSC as a deformable power source. The fabricated MSCs operate stably under various mechanical deformations, including stretching, folding, twisting, and wrinkling.

The demand of deformable energy storage systems (ESSs) is rapidly increasing for operating soft electronics<sup>1–7</sup>. In particular, for maximizing the functionality of soft electronics, efficient integration and space utilization of ESSs and electronic components are necessary<sup>8–13</sup>. In this regard, micro-supercapacitors (MSCs) have received much attention because of their efficient space utilization, customizable form factors, reliable electrochemical performance, and easy integration with electronic components<sup>14–20</sup>. The MSCs have been generally fabricated from in-plane rigid interdigitated current collectors on a substrate. However, the rigid current collectors fail mechanically and electrically even under a small mechanical deformation. In addition, the electrode materials on a rigid current collector easily crack and eventually peel off<sup>21,22</sup>. Therefore, to fabricate deformable MSC, a deformable electrode is necessary.

Designing the shape of solid electrodes such as fractal, kirigami, and serpentine patterns, has been considered an effective approach to achieving deformable MSCs<sup>6,23–27</sup>, because those patterns could accommodate a large mechanical deformation including the strain applied to the electrode. However, these approaches demand complicated fabrication process, such

as photolithography and vacuum deposition<sup>24,26,28,29</sup>. In addition, a large empty space between the electrode patterns should be required to accommodate mechanical deformation, which limits to fabricate a high density of the electrodes per unit area for high energy storage performance. A promising method to solve this problem is to use a liquid metal, for instance, EGaIn (eutectic gallium-indium alloy) as a current collector, because it possesses intrinsically liquid-phase characteristics, metallic conductivity, and self-healing property<sup>30–34</sup>. Zhang et al. prepared stabilized EGaIn ink by incorporating silk fibroin in EGaIn and used screen printing to produce a well-defined EGaIn current collector<sup>35</sup>. The obtained MSCs operated stably under mechanical deformations due to highly deformable EGaIn current collector. However, the fabrication of high-density interdigitated patterns with EGaIn remains a great challenge due to its high surface tension<sup>36,37</sup>. Since the energy storage performance of MSCs strongly depends on the areal density of the interdigitated electrodes, the gap between neighboring interdigitated electrodes should be minimized as long as the electrodes maintain the mechanical and electrical stability under mechanical deformation.

<sup>1</sup>National Creative Research Initiative Center for Hybrid Nano Materials by High-level Architectural Design of Block Copolymer, Department of Chemical Engineering, Pohang University of Science and Technology (POSTECH), Pohang, Gyeongbuk 37763, Republic of Korea. <sup>2</sup>Advanced Nano-Surface & Wearable Electronics Research Laboratory, Heat and Surface Technology R&D Department, Korea Institute of Industrial Technology, Incheon 21999, Republic of Korea. <sup>3</sup>Division of Chemical Engineering, Konkuk University, Seoul 05029, Republic of Korea. <sup>4</sup>Department of Materials Science and Engineering, Pohang University of Science and Technology (POSTECH), Pohang, Gyeongbuk 37763, Republic of Korea. <sup>5</sup>These authors contributed equally: Keon-Woo Kim, Seong Ju Park.  
✉ e-mail: [jkim@postech.ac.kr](mailto:jkim@postech.ac.kr); [chanu@kitech.re.kr](mailto:chanu@kitech.re.kr)

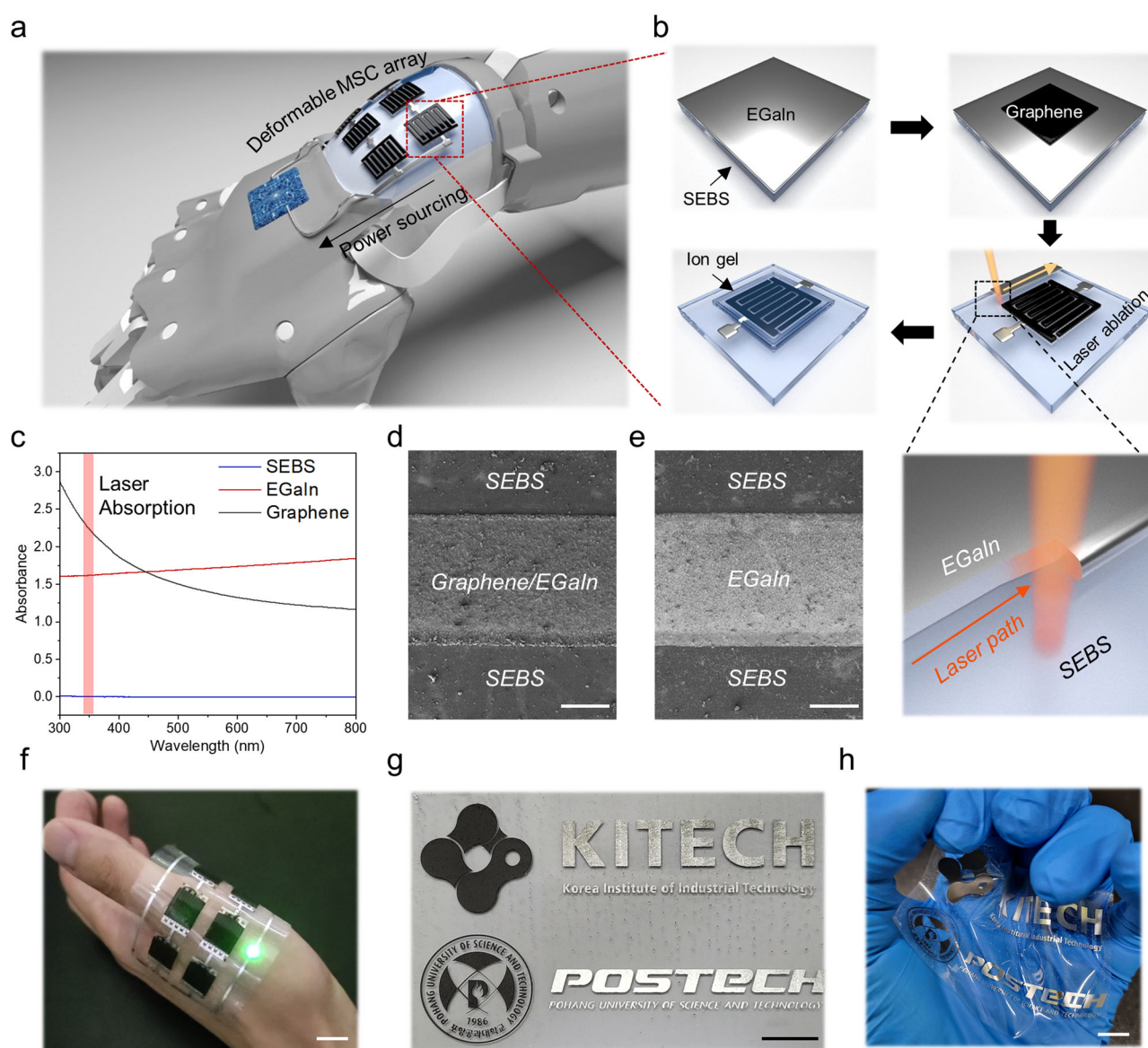
In this work, we fabricated deformable MSCs based on an EGaIn current collector, utilizing laser ablation technology. Graphene and polystyrene-*block*-poly(ethylene-co-butylene)-*block*-polystyrene copolymer (SEBS) were selected as an electrode and a flexible substrate, respectively. Due to a high weight percentage (70%) of the rubbery block (EB) in SEBS, SEBS accommodates a large strain or mechanical deformation. EGaIn film with a uniform thickness was fabricated on the SEBS substrate through a brushing method. Graphene was then coated onto the EGaIn film, and an interdigitated graphene/EGaIn electrode was fabricated using a laser ablation. During laser irradiation, graphene and EGaIn strongly absorbed the laser light at a wavelength (355 nm), while SEBS did not, providing selective ablation of graphene/EGaIn without loss of the flexibility of the SEBS. By judicious control of the gap of neighboring interdigitated electrodes and mass loading of graphene, we obtained a high electrochemical performance: a high areal capacitance ( $1336 \mu\text{F cm}^{-2}$ ), a good rate performance, and an excellent cycle stability ( $>10,000$  cycles). Furthermore, we fabricated a soft electronic system by integrating an MSC array and commercial

light-emitting diodes (LEDs) to demonstrate the potential application as a deformable ESS. The device stably operated under various mechanical deformations (e.g., stretching, twisting, folding, and clumping).

## Results and discussion

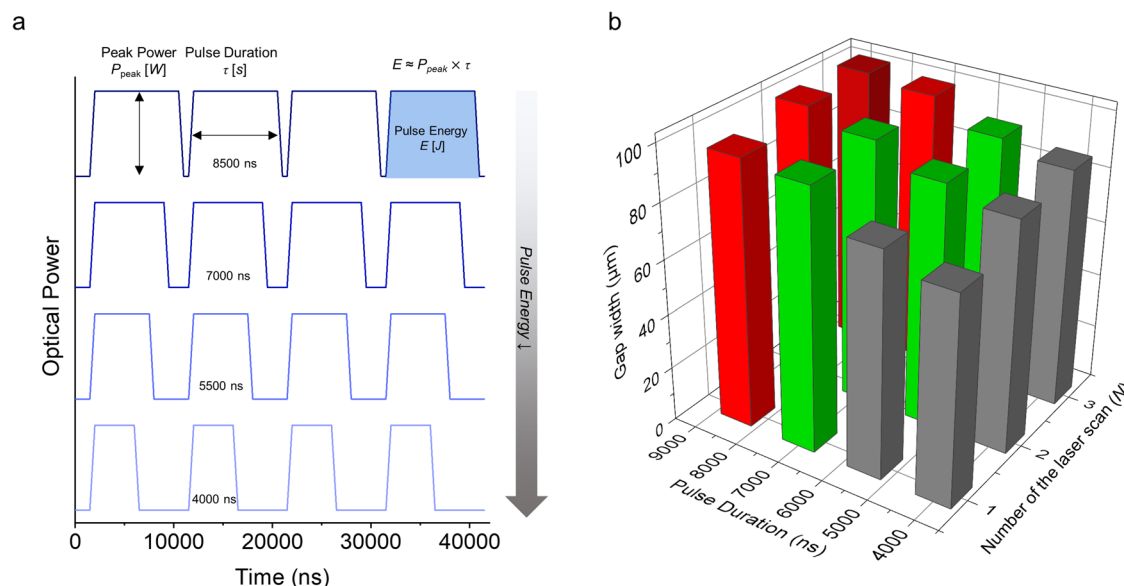
### Fabrication process for deformable micro-supercapacitors

Figure 1a shows an illustration of integrated soft electronic system, comprising deformable MSC array and wearable electronic device. Deformable MSC array is prepared as follows. First, EGaIn was coated onto the SEBS substrate using a brush (Fig. 1b). Despite the high surface tension of EGaIn, a uniform EGaIn film was obtained after brushing. The resulting EGaIn film exhibits excellent electrical properties, which is effectively used as a current collector (Supplementary Fig. 1). Then, graphene was selectively deposited onto desired regions of EGaIn film by screen-printing of graphene paste with a pre-designed stencil (Supplementary Fig. 2), resulting in graphene/EGaIn bi-layer (Fig. 1b). Next, a laser is irradiated along the pre-designed path to



**Fig. 1 | Fabrication process for deformable micro-supercapacitors.** **a** Illustration of an integrated system comprising soft-electronics and deformable energy storage component. **b** The fabrication process of EGaIn-based MSC. **c** UV-vis spectra of

SEBS, EGaIn, and graphene. FE-SEM images of laser ablated **d** Graphene/EGaIn and **e** EGaIn (Scale bar = 200  $\mu\text{m}$ ). Photographs of **f** institute logos, **g** deformed logos, and **h** an LED connected to the MSC circuit (Scale bar = 1 cm).



**Fig. 2 | Laser ablation optimization.** **a** Pulse energy dependence on the pulse duration. **b** Sample state after laser ablation as functions of pulse duration and the number of the laser scan (red region: damaged SEBS, green region: the entire ablation

of both graphene and EGaIn without any damage on SEBS, and gray region: only graphene ablation but not EGaIn).

fabricate the pattern. When the laser is irradiated, graphene/EGaIn and EGaIn along the path of the laser are ablated, resulting in interdigitated graphene/EGaIn pattern and EGaIn circuit, respectively. On the other hand, the laser does not affect the SEBS substrate because it barely absorbs the laser wavelength (355 nm) (Fig. 1c); thus the deformable characteristics of SEBS substrate is maintained. Then, poly(vinylidene fluoride-co-hexafluoropropylene) based ion gel was coated onto the interdigitated electrode region to complete MSCs. The field-emission scanning electron microscopy (FE-SEM) images of the laser ablated graphene/EGaIn and EGaIn are shown in Fig. 1d, e, respectively. An LED was connected to the MSC circuit (Fig. 1f). In addition, various deformable patterns on graphene/EGaIn and EGaIn were easily fabricated on the SEBS, e.g., the institute logo (Fig. 1g) which accommodates easily a large mechanical deformation (Fig. 1h).

### Optimization of laser ablation conditions

Even though SEBS barely absorbs the laser wavelength (355 nm), the heat generated during the laser ablation of graphene and EGaIn could potentially affect the SEBS. In addition, an intense laser could potentially cause damage to the SEBS. Consequently, we optimized the laser ablation process to ensure the complete ablation of both graphene and EGaIn without any damage on the SEBS. Figure 2a illustrates pulse energy ( $E$ ) change with pulse duration ( $\tau$ ). Here, we fixed the peak power ( $P_{\text{peak}}$ ) and laser frequency at 3.9 W and 100 kHz, respectively, while  $\tau$  was adjusted from 8500 ns to 4000 ns. Because  $E \approx P_{\text{peak}} \cdot \tau^{38,39}$ ,  $E$  decreases with reducing  $\tau$  at fixed  $P_{\text{peak}}$ . Figure 2b shows the state of the sample after laser ablation at different  $\tau$  and the number ( $N$ ) of the laser scan. The corresponding optical microscopy (OM) images are shown in Supplementary Fig. 3. Despite a very low laser absorption of the SEBS, a long pulse duration ( $\tau = 8500$  ns) caused severe damages (burned and even cut) on the SEBS (Supplementary Fig. 4). Regardless of  $N$ , the gap size after laser ablation decreases with decreasing  $\tau$ . When  $\tau$  is shorter than 7000 ns with a single scan, only graphene undergoes ablation, but EGaIn does not remove. On the other hand, at  $N = 2$  and 3, a complete EGaIn ablation was achieved even at  $\tau = 5500$  ns. We conclude that two scans of a laser with  $\tau$  of 5500 ns is the optimal condition, where there is no damage on the SEBS and the narrowest gap size ( $\sim 90$   $\mu\text{m}$ ) is achieved. This value is much smaller than that ( $\sim 1000$   $\mu\text{m}$ ) reported in the literature on printed EGaIn-based MSCs<sup>35,40</sup>.

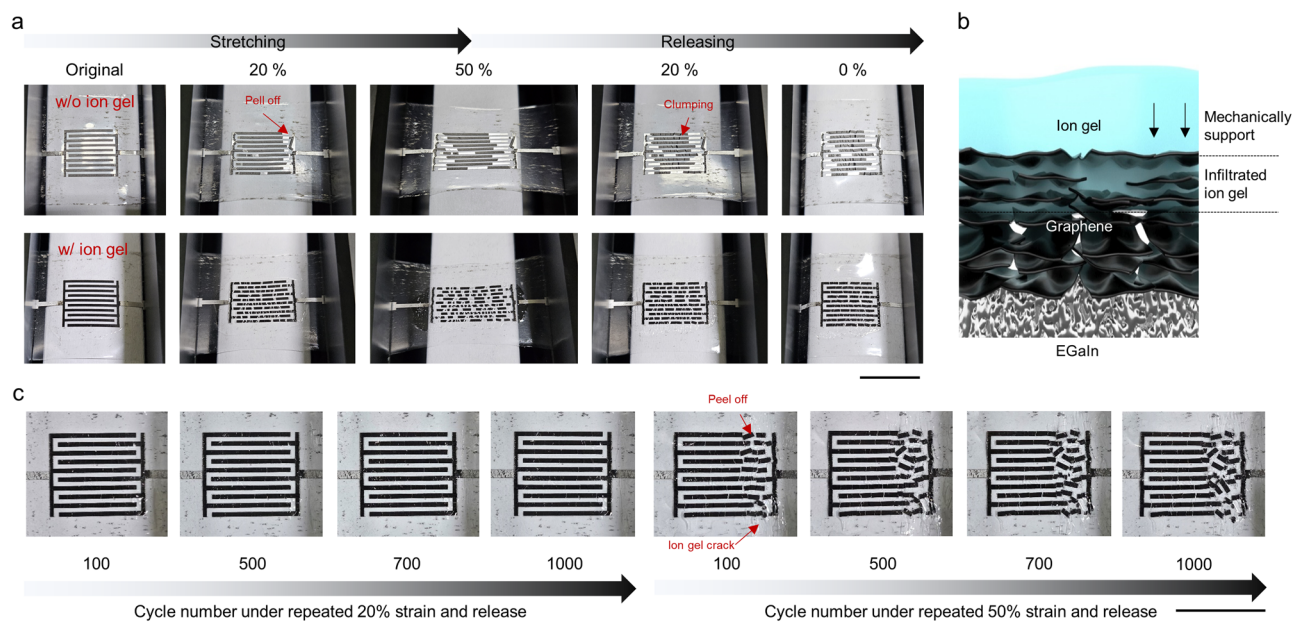
### Mechanical stability of EGaIn/Graphene electrode

Figure 3a shows photographs of graphene/EGaIn electrode during a single stretching and releasing at two different strains (20 and 50%) without and with the ion gel. In the absence of the ion gel, several large cracks were generated in the graphene layer during stretching regardless the strain, causing the graphene layer to clump and lose its original shape during the releasing process. Furthermore, the cracked graphene even peeled off from the EGaIn layer at 50% strain. This is attributed to a large difference in the tensile modulus between the brittle graphene layer and the EGaIn layer. On the other hand, in the presence of the ion gel, small cracks occurred uniformly in the graphene layer during stretching regardless strain. Nevertheless, the graphene layer was almost restored to its original shape except the trace of the cracks. This is attributed to the partial infiltration of the soft ion gel into the graphene layer (Fig. 3b), providing reliable adhesion to the EGaIn layer. Furthermore, there was no peeling off of the graphene layer even after 1000 cycles of repeated 20% stretching, indicating that the ion gel maintained a stable mechanical interface with the EGaIn layer (Fig. 3c). However, when stretching increases to 50%, a cracking occurred in the ion gel layer (Supplementary Fig. 5), causing the graphene layer to lose its original shape and eventually delaminate even after 100 cycles. Therefore, we conclude that a stable charge transport between graphene and EGaIn can be maintained up to 20% stretching.

### Tailoring gap size of MSCs

Because the rate performance and areal capacitance of the MSCs strongly depend on the gap size between neighboring interdigitated electrodes, we prepared three gap sizes (100, 180, and 500  $\mu\text{m}$ ) by adjusting a laser ablation path. Figure 4a shows the photograph of the fabricated MSCs with different gap sizes. Hereafter, the samples were denoted based on the gap size. For example, 500-MSC corresponds to MSC with a gap size of 500  $\mu\text{m}$ . Electrochemical impedance spectroscopy (EIS) was performed at a frequency ranging from 100 kHz to 10 mHz. According to the Nyquist plots shown in Fig. 4b, as the gap size decreases, the slope in the low-frequency region increases, which means better ion diffusion kinetics within the electrode materials. The diffusion coefficient ( $D$ ) of lithium ion calculated from the Warburg region (inset of Fig. 4b) for 100, 180, and 500-MSC is  $2.02 \times 10^{-4}$ ,  $6.21 \times 10^{-5}$ , and  $3.05 \times 10^{-5}$   $\text{cm}^2 \text{s}^{-1}$ , respectively. We also investigated the dependence of phase angle on the frequency of all MSCs (Fig. 4c). The relaxation time constant ( $\tau_0$ ) of MSCs, which is the minimum time required





**Fig. 3 | Mechanical stability against stretching and releasing of graphene/EGaIn electrode.** **a** Photographs of graphene/EGaIn electrode during a single stretching and releasing at two different strains (20% (left) and 50% (right)) without and with the ion gel (Scale bar = 1 cm). **b** Schematic of the roles of the ion gel during

mechanical stretching. **c** Photographs of graphene/EGaIn electrode during repeated stretching and releasing at two different strains (Scale bar = 1 cm) (20% (left) and 50% (right)).

to completely discharge all the stored energy with an efficiency of over 50%, is calculated as the inverse of the characteristic frequency ( $f_0$ ) (that is, the frequency at a phase angle of  $45^\circ$ ). The value of  $\tau_0$  for 500, 180, and 100-MSC are 6.3, 4.0, and 2.0 ms, respectively, suggesting faster ion kinetic with decreasing gap size.

To investigate the electrochemical behavior of the MSCs, we measured the cyclic voltammogram (CV) curves at  $50 \text{ mV s}^{-1}$  (Fig. 4d). The CV curves of all MSCs exhibit a quasi-rectangular shape, indicating electric double layer (EDL) behavior arising from adsorption/desorption of ions into graphene layers<sup>40</sup>. The curves widened as the gap size decreased, suggesting that MSCs with smaller gap sizes can store more charges. This is simply because the loading amount of graphene per unit area increases with decreasing gap size. This behavior is also confirmed in galvanostatic charging/discharging (GCD) profiles (Fig. 4e). As the gap size decreased, the charging/discharging duration of the GCD profiles increased without distorting the symmetrical shape. Based on the GCD curves at various current densities (Supplementary Fig. 6), the areal capacitance at a current density of  $2 \mu\text{A cm}^{-2}$  of 100-MSC was  $328 \mu\text{F cm}^{-2}$ , which is higher than those of 180-MSC ( $160.8 \mu\text{F cm}^{-2}$ ) and 500-MSC ( $78.24 \mu\text{F cm}^{-2}$ ). Moreover, 100-MSC maintained 77% areal capacitance even at a 15-fold higher current density ( $30 \mu\text{A cm}^{-2}$ ), showing a superior rate capability compared to 180 and 500-MSCs, which retained only 37.6 and 29.9%, respectively (Fig. 4f).

### Tailoring electrode thickness of MSCs

To further enhance the areal capacitance of 100-MSC, we controlled the graphene mass loading by multiple coating graphene paste (Supplementary Fig. 7). The MSCs were denoted on the basis of the number of the graphene layer ( $n$ ). For example, 3L-100-MSC is composed of a 3-layer graphene film with a gap size of the interdigitated pattern having 100  $\mu\text{m}$ . As  $n$  increased, the current increased at a given scan rate ( $50 \text{ mV s}^{-1}$ ), while the CV curves are slightly distorted (Fig. 4g). This is since the horizontal graphene sheet alignment results in low out-of-plane electrical conductivity and the resistance on the graphene film increases with increasing film thickness<sup>41</sup>. This is also supported by Nyquist plots in Fig. 4h. The semicircle in the high-frequency region was enlarged with increasing  $n$ , which is attributed to higher charge transfer resistance. Based on the measured GCD profiles at various current densities (Supplementary

Fig. 8), the areal capacitance was extracted (Fig. 4i). The 3L-100-MSC exhibited the areal capacitance of  $1336$  at  $2 \mu\text{A cm}^{-2}$  and  $705 \mu\text{F cm}^{-2}$  at  $30 \mu\text{A cm}^{-2}$ . Also, the value at all current densities are higher than others (2L-100-MSC and 1L-100-MSC). But, the rate capability (52.7%) of 3L-100-MSC is lower than others (69.1% of 2L-100-MSC and 77.0% of 1L-100-MSC). This is because, with increasing electrode thickness of MSCs, a large amount of charge could be stored in the device, but the inefficient electron transport through the entire electrodes makes the rate performance poor. Nonetheless, owing to the narrow gap size of the 3L-100-MSC, a better rate performance could be achieved compared to MSCs with one layer but a large gap (1L-500-MSC (29.9%) and 1L-180-MSC (37.6%)). Also, a long cycle life for practical application was achieved (Supplementary Fig. 9). A decrease of only 9.5% of the first run was recorded after 10,000 cycles.

### MSCs operation under mechanical deformations

The major requirement for a deformable energy storage device is to maintain the energy storage performance under various mechanical deformations. In this study, folding and stretching are selected for 3L-100-MSC for the deformability test (Fig. 5a). Figure 5b shows the CV curves under folding and 20% stretch. The CV curves under both cases remain almost the same, indicating the stable electrochemical behavior under mechanical deformation. Moreover, the GCD curves measured under mechanical deformations showed almost the same as that without deformation (Fig. 5c). Figure 5d compares the areal capacitance as a function of the current density under different deformation states, demonstrating that excellent performance stability (95 and 91% under folding and stretching, respectively). To operate deformable electronics reliably, energy storage components should maintain the energy storage performance not only in the deformed state but also after recovery state. We performed the cycle test with repetitive deformations (Fig. 5e). Regardless of the deformation type, we observed  $\sim 90\%$  capacitance retention after 1000 cycles, indicating that interdigitated graphene/EGaIn electrode on the SEBS sufficiently accommodated repetitive mechanical deformation and recovery. During repeated stretching and releasing at 20% strain, the small cracks and clumped region occurred at both the ion gel and the graphene layer. These structural deformations probably reduce the electrochemical properties (Supplementary Fig. 10). Thus, we believe

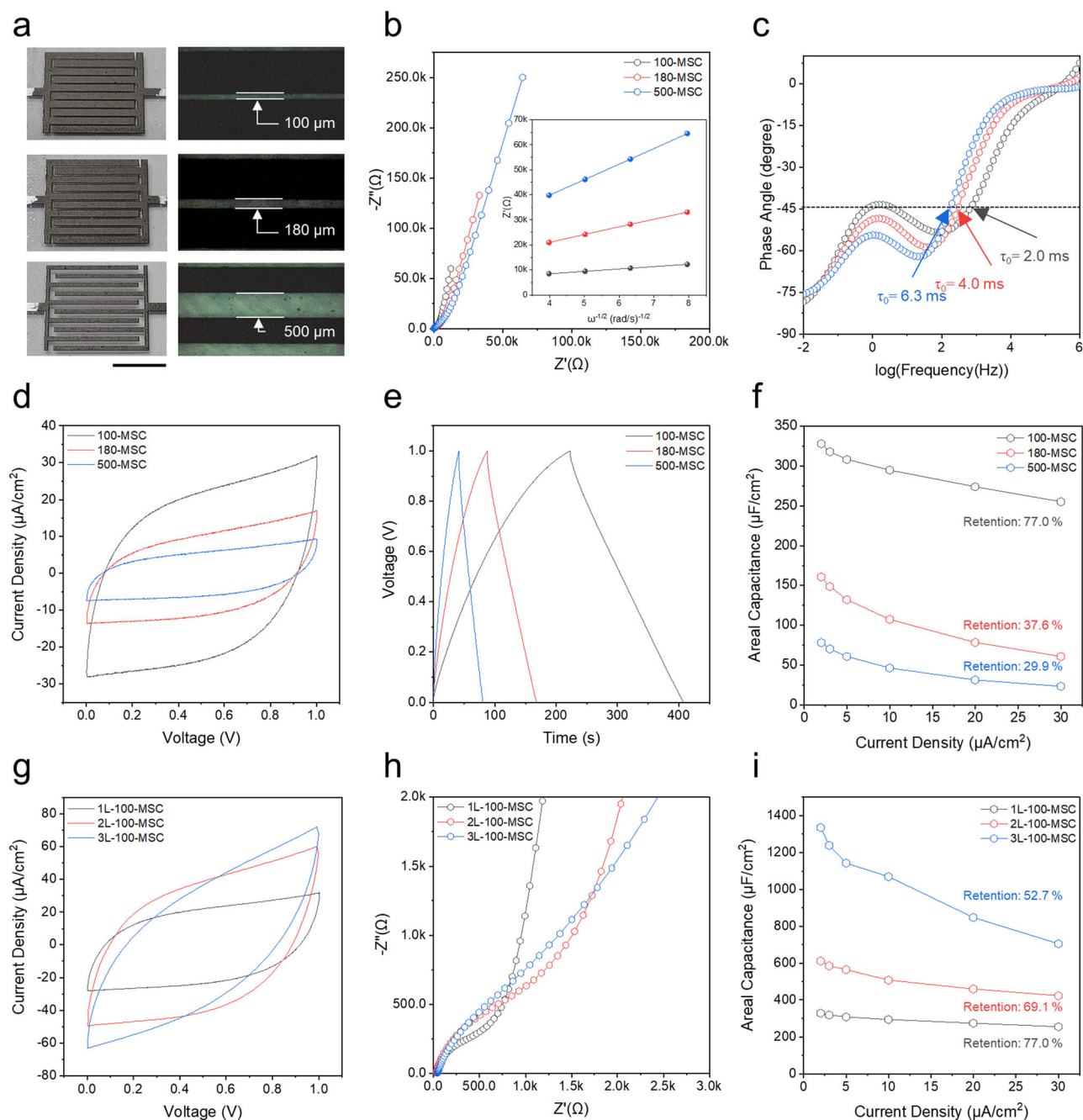


**Fig. 4 | Energy storage performance of MSCs.** **a** Photographs and OM images of three MSCs with different gap sizes (Scale bar = 5 mm). **b** Nyquist plots of MSCs. (inset:  $Z'$  as a function of  $\omega^{-1/2}$  plot in low frequency range). **c** Bode angle plots of MSCs. **d** CV curves of MSCs at  $50 \text{ mV s}^{-1}$ . **e** GCD curves of MSCs at  $2 \mu\text{A cm}^{-2}$ .

**f** Areal capacitances in the current density range from 2 to  $30 \mu\text{A cm}^{-2}$ . **g** CV curves of MSCs based on different graphene layers. **h** Nyquist plots of MSCs. **i** Areal capacitance vs current density of MSCs based on different graphene layers.

that the cycle stability of MSCs can be further improved by employing the mechanically durable ion gel.

### MSC array integration with electronics

To demonstrate MSC as a power source for a soft electronic system, we integrated the MSC array with LEDs (Fig. 6a). To meet the LED's operating voltage requirement and stable operation, we designed an MSC array consisting of 3 series and 3 parallel connections. To this end, we coated EGaIn on a large-area SEBS substrate and partially loaded graphene on coated EGaIn through screen printing. Next, nine interdigitated electrodes and the EGaIn circuits connecting them were prepared using laser ablation. Finally, MSC array was completed

by coating ion gel on the interdigitated electrode area. The area of fabricated MSC array was  $35 \text{ cm}^2$  ( $7 \text{ cm} \times 5 \text{ cm}$ ). The MSC array exhibited a wide CV curve and a 3-fold increase in operating voltage compared to a single arrayed MSC (Fig. 6b). Moreover, the shape of CV curve does not show any distortion, indicating stable electrochemical behavior. Figure 6c shows the GCD profiles of single MSC and MSC array. MSC array showed a 3-fold increase in charging/discharging duration and operating voltage, implying increased output energy and power (Fig. 6c). These results indicate that laser ablation enables a facile fabrication of MSC array in a large area (Supplementary Fig. 11). In addition, the high conductivity of the EGaIn current collector was achieved even though it was fabricated by

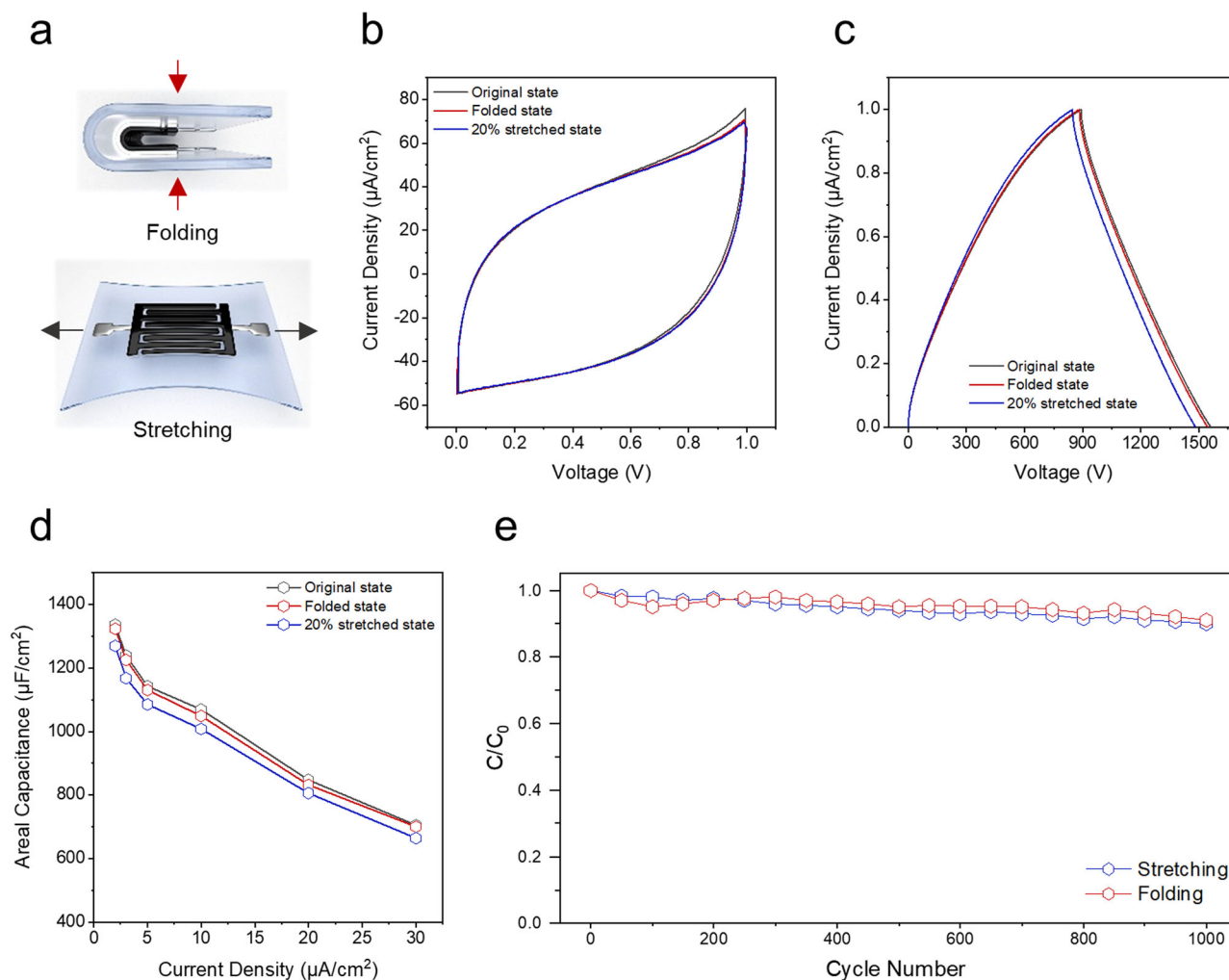


**Fig. 5 | The energy storage performance under various mechanical deformations.** **a** Photographs of MSC under various mechanical deformations. **b** CV curves and **c** GCD profiles under different mechanical deformations. **d** Areal capacitance. **e** Capacitance retention with repetitive mechanical deformations.

brushing method to cover a large device area. Finally, when two LEDs were connected to the MSC array through the EGaIn circuit, they stably operated under various mechanical deformations, including stretching, twisting, folding, and wrinkling (Fig. 6d). Furthermore, even with just two MSCs connected in series, various electronics could be operated (Supplementary Fig. 12).

### Miniaturization of MSCs

Utilizing the high-resolution patterning capability of laser ablation, we successfully downsized the MSCs. While maintaining a gap size, we fabricated smaller MSCs with total sizes of 0.5 cm<sup>2</sup> and 0.25 cm<sup>2</sup> (Fig. 6e). As the gap size remained constant, the amount of loaded graphene on per unit area is identical. Consequently, all samples exhibited nearly identical electrochemical behaviors (similar CV curves) (Fig. 6f). Moreover, almost identical charging/discharging durations were observed regardless of MSC size (Fig. 6g), indicating the reliable energy storage performance of downsized MSCs. Lastly, we demonstrated the operation of an LED by using three serially connected MSC units of a downsized area (0.5 cm<sup>2</sup>) under bending (Fig. 6h).

In summary, we fabricated deformable MSCs by using laser ablation technique. To optimize the energy storage performance, we tailored the gap size of the interdigital electrodes and the mass loading of graphene. The fabricated MSC exhibited a high areal capacitance

(1336 μF cm<sup>-2</sup>) with reliable rate performance. Remarkably, the MSC retained the energy storage performance under various mechanical deformations due to the intrinsic liquid state of EGaIn current collector and the highly flexibility of SEBS substrate. To demonstrate the feasibility of MSCs as a deformable power source, we fabricated a soft electronic system comprising serial and parallel connected MSC array and LEDs. The obtained soft electronic system stably operated under various mechanical deformations (e.g., folding, stretching, wrinkling, and twisting). To increase further the stretching of MSCs, a highly mechanical durable ion gel such as polystyrene-*b*-poly(-methylmethacrylate)-*b*-polystyrene copolymer is desirable. As the laser ablation technology can easily be utilized to pattern various electrode materials including carbon materials, metal oxides, and Mxene, this could be applied for highly deformable and high-performance energy storage systems.

### Methods

#### Materials

All chemicals were purchased from Sigma-Aldrich, except graphene paste, which was from MExplorer Co Ltd. To prepare a deformable substrate, SEBS powder (2 g) was dissolved to toluene (10 g). Thereafter, the obtained solution was coated on a glass using a blade coater. Subsequently, the SEBS-coated glass was placed in an oven at 100 °C for 30 m to evaporate solvent. The fabricated SEBS film



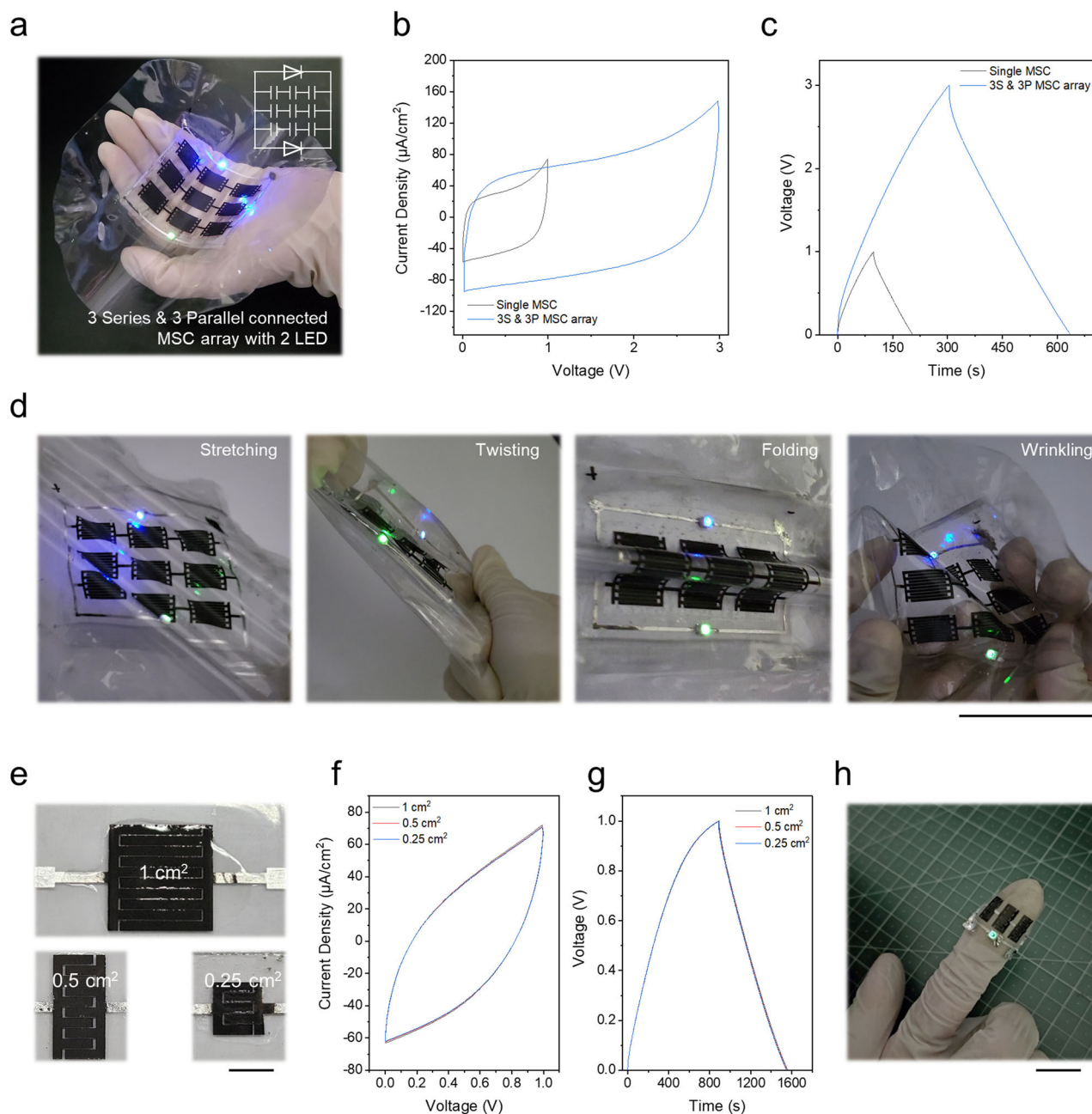


**Fig. 6 | Fabrication of MSC array and miniaturization of MSC.** **a** Photograph of nine MSC units connected in three parallel and three series. **b** CV curves and **c** GCD profiles of single MSC and multiple MSC array. **d** Photographs of the MSC array integrated with two LEDs circuit under various mechanical deformations (Scale

bar = 5 cm). **e** Photographs of the downsized MSC units (Scale bar = 0.5 cm). **f** CV curves at 50 mV/s and **g** GCD profiles at 2  $\mu\text{A}/\text{cm}^2$  of the downsized MSCs.

**h** Photograph of three serially connected MSC units of a downsized area ( $0.5 \text{ cm}^2$ ) integrated with LED circuit under bending (Scale bar = 2 cm).

was easily peeled off from the glass and used as a deformable substrate.

### Device fabrication

EGaIn was first coated onto the SEBS substrate using a brush painting. Next, a graphene paste was selectively coated onto the desired region by screen-printing with pre-designed stencil and dried at 70 °C for 1 h. Multiple layered graphene with a high thickness was prepared by multiple printing. Lastly, a UV pulsed laser with a wavelength of 355 nm was irradiated to the interdigitated electrodes. To prepare the ion gel electrolyte, poly(vinylidene fluoride-co-hexafluoropropylene) [P(VDF-co-HFP)] and 1-ethyl-3-methylimidazolium bis-(trifluoromethylsulfonyl)imide [EMI][TFSI] were dissolved in acetone at

a predetermined weight ratio of 1:9. The obtained ion gel solution was solution casted onto the interdigitated electrode region and dried to form the gel state at 50 °C for 30 min to complete the flexible MSC device.

### Characterization

Laser patterned electrodes were characterized by FE-SEM (S-4800, Hitachi) and OM (BX51M, Olympus). Transmittance spectra were recorded on a UV-vis spectrometer (UV-2550, Shimadzu). Electrochemical measurements were conducted using a potentiostat (Weis 500, WonA Tech). Mechanical properties were measured using a folding tester (CFT-070i, COVOTECH) and a stretchable tester (CST-010K, COVOTECH).

## Data availability

The data that support the findings of this study are available from the corresponding author upon reasonable request.

Received: 12 October 2023; Accepted: 6 March 2024;

Published online: 14 March 2024

## References

- Wang, X. et al. High-performance stretchable supercapacitors based on intrinsically stretchable acrylate rubber/MWCNTs@conductive polymer composite electrodes. *J. Mater. Chem. A* **6**, 4432–4442 (2018).
- Niu, Z. et al. Highly stretchable, integrated supercapacitors based on single-walled carbon nanotube films with continuous reticulate architecture. *Adv. Mater.* **25**, 1058–1064 (2013).
- Park, S. et al. Stretchable energy-harvesting tactile electronic skin capable of differentiating multiple mechanical stimuli modes. *Adv. Mater.* **26**, 7324–7332 (2014).
- Kim, K.-W., Park, B., Kim, J., Jo, C. & Kim, J. K. Recent progress in block copolymer soft-template-assisted synthesis of versatile mesoporous materials for energy storage systems. *J. Mater. Chem. A* **11**, 7358–7386 (2023).
- Liu, Y.-H. et al. High-performance, ultra-flexible and transparent embedded metallic mesh electrodes by selective electrodeposition for all-solid-state supercapacitor applications. *J. Mater. Chem. A* **5**, 9032–9041 (2017).
- Yun, J. et al. A fractal-designed stretchable and transparent microsupercapacitor as a skin-attachable energy storage device. *Chem. Eng. J.* **387**, 124076 (2020).
- Kim, K.-W. et al. Extremely fast electrochromic supercapacitors based on mesoporous WO<sub>3</sub> prepared by an evaporation-induced self-assembly. *NPG Asia Mater.* **12**, 84 (2020).
- Wang, Y. & Xia, Y. Recent progress in supercapacitors: From materials design to system construction. *Adv. Mater.* **25**, 5336–5342 (2013).
- Kyeremateng, N. A., Brousse, T. & Pech, D. Microsupercapacitors as miniaturized energy-storage components for on-chip electronics. *Nat. Nanotechnol.* **12**, 7–15 (2017).
- García Núñez, C., Manjakkal, L. & Dahiya, R. Energy autonomous electronic skin. *npj Flex. Electron.* **3**, 1 (2019).
- Liu, N. & Gao, Y. Recent progress in micro-supercapacitors with in-plane interdigital electrode architecture. *Small* **13**, 1701989 (2017).
- Wang, J., Li, F., Zhu, F. & Schmidt, O. G. Recent progress in micro-supercapacitor design, integration, and functionalization. *Small Methods* **3**, 1800367 (2019).
- Kim, K.-W. et al. Electrostatic-force-assisted dispensing printing of electrochromic gels for low-voltage displays. *ACS Appl. Mater. Interfaces* **9**, 18994–19000 (2017).
- Lethien, C., Le Bideau, J. & Brousse, T. Challenges and prospects of 3D micro-supercapacitors for powering the internet of things. *Energy Environ. Sci.* **12**, 96–115 (2019).
- Beidaghi, M. & Gogotsi, Y. Capacitive energy storage in micro-scale devices: Recent advances in design and fabrication of micro-supercapacitors. *Energy Environ. Sci.* **7**, 867–884 (2014).
- Chmiola, J., Largeot, C., Taberna, P.-L., Simon, P. & Gogotsi, Y. Monolithic carbide-derived carbon films for micro-supercapacitors. *Science* **328**, 480–483 (2010).
- Pech, D. et al. Ultrahigh-power micrometre-sized supercapacitors based on onion-like carbon. *Nat. Nanotechnol.* **5**, 651–654 (2010).
- El-Kady, M. F. & Kaner, R. B. Scalable fabrication of high-power graphene micro-supercapacitors for flexible and on-chip energy storage. *Nat. Commun.* **4**, 1475 (2013).
- Chu, X., Yang, W. & Li, H. Recent advances in polyaniline-based micro-supercapacitors. *Mater. Horiz.* **10**, 670–697 (2023).
- Chu, X. et al. Air-stable conductive polymer ink for printed wearable micro-supercapacitors. *Small* **17**, 2100956 (2021).
- Rogers, J. A., Someya, T. & Huang, Y. Materials and mechanics for stretchable electronics. *Science* **327**, 1603–1607 (2010).
- Kim, M.-G. et al. All-soft supercapacitors based on liquid metal electrodes with integrated functionalized carbon nanotubes. *ACS Nano*. **14**, 5659–5667 (2020).
- Lim, Y. et al. Biaxially stretchable, integrated array of high performance microsupercapacitors. *ACS Nano*. **8**, 11639–11650 (2014).
- Kim, D., Shin, G., Kang, Y. J., Kim, W. & Ha, J. S. Fabrication of a stretchable solid-state micro-supercapacitor array. *ACS Nano*. **7**, 7975–7982 (2013).
- Yun, J. et al. Stretchable patterned graphene gas sensor driven by integrated micro-supercapacitor array. *Nano Energy* **19**, 401–414 (2016).
- Jiao, S., Zhou, A., Wu, M. & Hu, H. Kirigami patterning of mxene/bacterial cellulose composite paper for all-solid-state stretchable micro-supercapacitor arrays. *Adv. Sci.* **6**, 1900529 (2019).
- Zhang, C. et al. High-energy all-in-one stretchable micro-supercapacitor arrays based on 3d laser-induced graphene foams decorated with mesoporous znp nanosheets for self-powered stretchable systems. *Nano Energy* **81**, 105609 (2021).
- Xu, S. et al. Stretchable batteries with self-similar serpentine interconnects and integrated wireless recharging systems. *Nat. Commun.* **4**, 1543 (2013).
- Zhang, Y., Huang, Y. & Rogers, J. A. Mechanics of stretchable batteries and supercapacitors. *Curr. Opin. Solid State Mater. Sci.* **19**, 190–199 (2015).
- Daeneke, T. et al. Liquid metals: Fundamentals and applications in chemistry. *Chem. Soc. Rev.* **47**, 4073–4111 (2018).
- Chen, S., Wang, H.-Z., Zhao, R.-Q., Rao, W. & Liu, J. Liquid metal composites. *Matter* **2**, 1446–1480 (2020).
- Dickey, M. D. Stretchable and soft electronics using liquid metals. *Adv. Mater.* **29**, 1606425 (2017).
- Kazem, N., Hellebrekers, T. & Majidi, C. Soft multifunctional composites and emulsions with liquid metals. *Adv. Mater.* **29**, 1605985 (2017).
- Dickey, M. D. et al. Eutectic gallium-indium (egain): A liquid metal alloy for the formation of stable structures in microchannels at room temperature. *Adv. Funct. Mater.* **18**, 1097–1104 (2008).
- Zhang, Y. et al. Highly conductive egain/silk fibroin ink for graphene 3D array structure micro-supercapacitors. *Chem. Eng. J.* **428**, 132084 (2022).
- Li, X. et al. Evaporation-induced sintering of liquid metal droplets with biological nanofibrils for flexible conductivity and responsive actuation. *Nat. Commun.* **10**, 3514 (2019).
- Zhang, W., Chen, J., Li, X. & Lu, Y. Liquid metal-polymer microlattice metamaterials with high fracture toughness and damage recoverability. *Small* **16**, 2004190 (2020).
- Lee, H.-L., Hussain, A., Moon, Y.-J., Hwang, J. Y. & Moon, S. J. Influence of pre-sintering on the nanosecond pulsed laser ablation patterns of spin-coated silver nanoparticles. *Appl. Phys. A* **129**, 705 (2023).
- Miotello, A. & Kelly, R. Laser-induced phase explosion: New physical problems when a condensed phase approaches the thermodynamic critical temperature. *Appl. Phys. A* **69**, S67–S73 (1999).
- Yang, J. et al. Stretchable multifunctional self-powered systems with Cu-EGaln liquid metal electrodes. *Nano Energy* **101**, 107582 (2022).
- Kim, K.-W. et al. Soft template-assisted fabrication of mesoporous graphenes for high-performance energy storage systems. *ACS Appl. Mater. Interfaces* **14**, 46994–47002 (2022).

## Acknowledgements

This research was supported by the Industry-leading Core Production Technology Development Project of the Korea Institute of Industrial Technology (KITECH), and granted financial resources from the Ministry of Economy and Finance, Republic of Korea (No. EO240009). This work was



supported by the National Creative Research Initiative Program supported by the National Research Foundation of Korea (NRF) grant (no. 2022R1A3A3002149) funded by the Korean government.

### Author contributions

K.-W.K. and S.J.P. contributed equally to the work. K.-W.K. and S.J.P. designed the experiments. S.J.P. prepared the samples, and carried out the characterizations. K.-W.K. wrote the draft of the manuscript with the supervision of J.K.K. C.Y. helped with writing the draft of the manuscript. S.-J.P., I.K., and B.P. helped the experiments. S.H.K. and U.J. were involved in the discussions and manuscript revision. U.J. advised on the data analysis and result interpretation. J.K.K. and C.Y. managed the project and guided the research. All authors have read the approved the final paper.

### Competing interests

The authors declare no competing interests.

### Additional information

**Supplementary information** The online version contains supplementary material available at <https://doi.org/10.1038/s41528-024-00306-2>.

**Correspondence** and requests for materials should be addressed to Jin Kon Kim or Chanwoo Yang.

**Reprints and permissions information** is available at <http://www.nature.com/reprints>

**Publisher's note** Springer Nature remains neutral with regard to jurisdictional claims in published maps and institutional affiliations.

**Open Access** This article is licensed under a Creative Commons Attribution 4.0 International License, which permits use, sharing, adaptation, distribution and reproduction in any medium or format, as long as you give appropriate credit to the original author(s) and the source, provide a link to the Creative Commons licence, and indicate if changes were made. The images or other third party material in this article are included in the article's Creative Commons licence, unless indicated otherwise in a credit line to the material. If material is not included in the article's Creative Commons licence and your intended use is not permitted by statutory regulation or exceeds the permitted use, you will need to obtain permission directly from the copyright holder. To view a copy of this licence, visit <http://creativecommons.org/licenses/by/4.0/>.

© The Author(s) 2024